UCRL--93452

DE87 009136

DESIGN AND COMPONENT SPECIFICATIONS FOR HIGH AVERAGE POWER LASER OPTICAL SYSTEMS

R. W. O'Neil*, R. H. Sawicki*, S. A. Johnson* and W. C. Sweatt**

*Lawrence Livermore National Laboratory
P. O. Box 808
Livermore, California 94550

**Sandia National Laboratory
Albuquerque, New Mexico

Design and Component Specification for High Average Power Laser Optical Systems

By: R. W. O'Neil, R. H. Sawicki, S. A. Johnson, W. C. Sweatt

Laser imaging and transport systems are considered in the regime where laser-induced damage and/or thermal distortion have significant design implications. System design and component specifications are discussed and quantified in terms of the net system transport efficiency and phase budget. Optical substrate materials, figure, surface roughness, coatings, and sizing are considered in the context of visible and near-IR optical systems that have been developed at Lawrence Livermore National Laboratory for laser isotope separation applications. In specific examples of general applicability, details of the bulk and/or surface absorption, peak and/or average power damage threshold, coating characteristics and function, substrate properties, or environmental factors will be shown to drive the component size, placement, and shape in high-power systems. To avoid overstressing commercial fabrication capabilities or component design specifications, procedures will be discussed for compensating for aberration buildup, using a few carefully placed adjustable mirrors. By coupling an aggressive measurements program on substrates and coatings to the design effort, an effective technique has been established to project high-power system performance realistically and, in the process, drive technology developments to improve performance or lower cost in large-scale laser optical systems.

Work performed under the auspices of the U.S. Department of Energy by Lawrence Livermore National Laboratory under Contract W-7405-ENG-48.

Introduction

During the last 25 years, visible lasers have evolved from milliwatts of output power with marginal propagation properties to several hundred watts, near diffraction-limited systems. The stress placed on optical-systems designers to preserve the power and quality of higher-power laser beams has increased significantly. In this paper we will describe a thermo-optical system design approach we have used at Lawrence Livermore National Laboratory (LLNL) to construct a large scale Atomic Vapor Laser Isotope Separation system (AVLIS), called the Laser Demonstration Facility (LDF).[1,2] Figure 1 is an artist's rendering of the LDF, described recently at the CLEOS meeting in Baltimore, that illustrates the modular laser-optical architecture of this system.[3] Many copper-laser oscillator amplifier chains, operating at high pulse-repetition frequency (>4 kHz), are used to pump tunable dye laser oscillator amplifier chains. Although this high average power (presently hundreds and later thousands of watts) system contains over 3000 pieces of optics, the basic optical architecture can be broken down into a number of relatively simple laser or optical imaging modules. In this paper a single imaging module will be examined from a thermo-optical point of view to illustrate a cost-effective technique for achieving overall system optimization.

The optical-design approach discussed below has evolved within the context of a general design philosophy appropriate to large-scale high average-power laser systems such as LDF. In the regime of small thermal distortion (<1 λ), laser-induced thermal effects are explicitly

included in an optical-performance optimization process. An experimentally generated material property data base is used to bound performance ranges that, in turn, generates criteria for choosing from among several options a particular optical-design configuration. If the designer is then free to readjust element spacings in the original low-power optical module configuration to minimize the hot optical path difference (OPD), most of the thermally induced aberrations can be reduced significantly. Experimentally, this process has been found to converge, in agreement with relatively low-resolution (approximate) analysis. Consequently this approach facilitates the design of distributed systems with a large number of surfaces. Also, since the aberration, other than sphere, that typically builds up most rapidly with numbers of components is astigmatism, a technique to compensate for undesired cylindrical curvatures is illustrated that has improved wavefront distortion in a system of ~60 surfaces from about ($\lambda/4$) rms to ($\lambda/15$) rms.

Design Approach

In an AVLIS system the optical system physically wires the lasers and the material-processing chamber together. Because laser photons are typically very expensive to generate, it is essential to design the most efficient and least expensive optical system possible. In the LDF system, a number of laser subsystems are combined in series-parallel paths chosen to minimize the number of components needed to deliver near diffraction-limited light to a process vessel. In the design of the

optical system, the following guidelines were employed:

- To minimize diffraction losses all light within the laser system is image relayed between its source and destination, or propagates only in the near field of the last aperture.
- To minimize active pointing-and-centering system requirements, imaging systems are designed with conjugate points at critical optical components and optical components are mounted on massive inertial structures to damp out external influences.
- To maximize optical-system performance and minimize aberrations, the F-number of powered components is typically large (>20).
- Chromatic and thermal aberrations are minimized by extensive use of reflective components.

Within these guidelines we will discuss the thermo-optical design of a typical imaging module to illustrate the relative high average-power performance of a refractive and a reflective visible laser imaging system, using presently available optical materials, coatings, and fabrication techniques. Table I lists the operational specifications for a specific optical-imaging module discussed later in this paper. These requirements are appropriate for a dye-laser imaging-relay system that could be used for absorption and damage tests on optical coatings and substrates.

In a typical AVLIS system the laser beam passes in series through 16 to 25 laser or optical modules. We attempt to design all modules to have less than $\pm 0.02\ \lambda$ residual peak geometric and thermal aberration. Fabrication tolerances are chosen that give a peak noncorrectable

wave-front error of less than $\pm 0.05\ \lambda$ over the effective aperture (EA). [Typically the EA is about 20% of the system clear aperture (CA) on nonflat optics.] Since the rms wave-front distortion is nearly always less than one third of the peak value, the total system aberration goal is to be less than $\lambda/15$ rms.

Realizing excellent optical quality in even simple laser imaging systems is not easy. Typically, very detailed analyses of each component, characterized by very precisely defined coating, substrate, environmental, and laser specifications, are employed to design a high-power laser-transport system. Ultimate system performance is usually dependent on how closely the fabricated specifications conform to those used to generate the designs. The coating absorption, substrate coefficient of thermal expansion (CTE), details of thermal paths in the optical mounts and surrounding environment, and the laser-beam quality frequently differ from design values. Thus, it is important to assess the impact of a range of key parameter values on the design goals. In this paper we will examine an approach that uses balanced tradeoffs of optical design and fabrication complexity with mechanical-design provisions to allow for active accommodation of small thermal distortions. From numerous design exercises it was found that within this framework the level of thermal/structural analysis of optical elements need be only approximate to achieve a high overall system performance. In many applications these calculations can be performed on desk-top computers, since the number of calculational steps in a finite-difference analysis scales quadratically with the number of nodes

employed in each component. In the AVLIS system design, we have found that an adequate thermo-structural analysis of a multielement optical system (>50 surfaces), coupled to an appropriate ray-trace code, can be performed rapidly enough to permit near real-time OPD optimization. Presently we are using Super-OSLO for optical analysis because of its ability to incorporate a user-supplied subroutine to modify inputs to the optical parameters.[4] These inputs are generated with a thermal/structural/optical code (TSO) developed at LLNL that calculates the thermally modified x and y components of the radii of curvature of as many as 200 elements as a function of their power loading and material properties.[5] The calculational response is rapid enough to conveniently use the full optimization capabilities of OSLO.

TSO - OSLO

Figure 2 illustrates the architecture of TSO-OSLO. First the cold optical system is designed within the guidelines outlined in Table I. Using the input power densities defined by these geometric spot sizes (assumed spatially uniform) and the measured surface and bulk absorption, transmittance, and other appropriate material properties, the temperature distribution and the associated structural and dn/dT optical changes are calculated in TSO. From the heat-transfer analysis, which can include radiation, convection, and conduction in most realizable boundary configurations, data are used to calculate effective x and y radii of curvature on each component. In an iterative manner the new curvatures

are automatically inputed to OSLO to recalculate the thermal loadings and, ultimately, the net optical-system distortion due to geometric and thermal factors. Typically only a few iterations are required to converge to a stable hot configuration. As indicated in Table I, the optical-system configuration was chosen to be independently adjustable in magnification and collimation, which makes it possible in all systems we have examined to make small readjustments in component spacing to minimize the net system OPD without having to recalculate the thermal characteristics.

TSO was developed to be a user-friendly code for optical designers not familiar with complex thermo-structural-analysis tools. Although the code can use up to 2000 nodal points to simulate heat transfer and the resulting optical distortions in each element, typically only a few hundred are required for most problems. (Adequacy was determined from detailed comparison with high-resolution finite-element analysis results.)

TSO assumes a nominally uniform bisymmetric (elliptical or rectangular) spatial distribution, but the code is reasonably accurate for all but the most pathological distributions, such as annular or strongly multimodal laser beams. Figure 3 is a plot of the thermally induced OPD in a radiatively and convectively cooled window, irradiated with (a) a uniform circular beam and (b) the Fresnel diffraction pattern of (a) propagated about half way to its far-field. As can be seen, the OPD is approximately spherical for both distributions and the difference from spherical is much less than 20% of the total OPD.

Material Properties

As illustrated in the logical flow in Fig. 2, the effectiveness of any thermal-design code is fundamentally limited by the availability and quality of the input data on coatings and substrate materials. Although some data can be found in handbooks or in the more current technical literature, applicable data on surface and bulk absorption of optical elements are generally very difficult to find. Also, since as-received optics performance depends upon the specific manufacturing techniques employed, the thermal analysis is sometimes based on nonrealizable component characteristics. To address this issue we at LLNL have developed a nonintrusive technique for measuring these key parameters that we are using for our analysis.[6] In addition, we have obtained from the Center for Laser Studies [University of Southern California, Los Angeles, California (USC)], a number of independent measurements on materials we used for substrate fabrication that were characterized using sensitive laser calorimetric techniques.[7,8] Over the last 10 years the bulk absorption and/or the measurement procedures used to establish the values of fused silica have been greatly improved. Figure 4 is a representative compilation of measurements on fused silica and sapphire from the literature, USC, and measurements made at LLNL.[9-12] As can be seen, the bulk absorption of presently available fused silica is approaching the fiber-optics limit of about 1 dB/km (10^{-6}/cm) at 1.06 μm and is less than 5×10^{-5}/cm at 600 nm, the lower limit used in our calculations. At 568 nm most of the presently available high-quality

fused silica from most vendors has similar values of bulk absorption. To compare different sources, 1-cm^2 samples were fabricated with rms surface roughness less than 10 Å. When measured calorimetrically, Suprasil W-1 has about half the absorption of Dynasil 1001. Ultrasil-2, Thermosil American, Corning 7940, Suprasil-2, and Dynasil 4101 fall between the minimum and maximum values of 3×10^{-5} and 6×10^{-5}, respectively.[8] In the visible, this low absorption more than compensates for the poor dn/dT of fused silica to make it one of the best transparent materials for average power system design. In some specific applications, particularly for pressure windows, sapphire can be a competitive material. Sapphire generally has higher bulk absorption, but it can usually be much thinner and have comparable thermal properties because of its very high thermal conductivity. Unfortunately, it is difficult to fabricate Al_2O_3 to the same figure and surface roughness (a factor in surface absorption) as fused silica, and thermally induced birefringence is sometimes a problem in polarized laser systems.

The thermal input data on mirror and lens materials used in the following examples are summarized in Table II.

Optical Coatings

Over the last 2 years there have been significant developments in high average power density low-absorption anti-reflection (AR) and moderate-bandwidth (±30 nm) maximum-reflectivity multilayer dielectric (MLD) visible coatings. Table II summarizes the typical range of coating

absorptions that has been achieved in optics purchased over the last year. As can be seen, the range of measured values is over an order of magnitude and any critical design task will require that representative optical elements be measured to define appropriate values for the high-power analysis. On specific coating designs manufactured in a limited number of coating chambers, several vendors have been able to deliver, reproducibly, several hundred pieces of optics in sizes up to 25 cm with the absorption values falling within a factor of 2 of the lowest we have seen ($<10^{-5}$). Reflectivities > 0.998 in a $\pm$30-nm band are fairly typical in these low-absorption designs. We have verified that these low-absorption reflective coatings are stable in even harsh environments but, as should be expected, only if they are maintained at near perfect cleanliness. The lowest absorption values are about 20 times smaller than any we had seen 2 years ago.

Multidielectric AR coatings around 600 nm are also very good. At 20 kW/cm^2 in a 0.04-cm-diam spot, typical temperature rises seen on fused silica windows due to surface absorption are much less than 1° C, corresponding to less than 10^{-5} surface absorption. Under the same irradiance conditions AR sol-gel coatings, developed at LLNL for very high peak power laser fusion applications, generate surface temperatures too small to be measured with 0.1° C sensitivity.[13] In this paper the range of values are appropriate to commercial MLD coatings.

Average power damage resistance of both AR and high-reflectivity coatings correlates well with the surface absorption, indicating a primary dependency on average power density, rather than fluence, the parameter of

interest for single-shot damage. Although there is little single-shot damage data on these low-absorption coatings at this time, practical operational average power design levels are typically 3 to 5 times lower than would be chosen from single-pulse fluence considerations in the 30 to 60 ns pulse-length regime. In a limited sample we have seen coating failure in most components heated more than a few tens of degrees by the laser beam. The majority of low-absorption coatings can operate continuously in our test facility (many hours) in high pulse-repetition frequency systems (>4 kHz), with 20 kW/cm^2 over small spots (~1 mm) with no indication of damage or deterioration.

Thermo-Optical Design

To meet the optical imaging goals of Table I, two optical configurations illustrated in Fig. 5 will be analyzed using the range of material values described above. The boundary conditions are defined in both configurations to have radiative and convective heat loss only to minimize overall optical distortion. The first refractive configuration [Fig. 5(a)] is a three-lens system that will easily meet all cold-system requirements. Lenses can be manufactured from either fused silica or sapphire to have the appropriate curvatures and also to have peak figure errors over the laser beam subaperture that are less than 0.05 λ

The second or reflective arrangement, [Fig. 5(b)] constructed from four Zerodur mirrors, has the same image and collimation control features and can achieve adequate, but slightly poorer quality, low-power optical

performance. This configuration is more complex (and expensive) and is more sensitive to background vibrations. Note, however, that this mirror arrangement does provide a convenient means to adjust the position and angle of the output beam. In the following discussion the relative high-power (thermal) performance of these two configurations will be compared for an incident average power of 500 W in a circular beam of uniform intensity. In the design the spot sizes will be chosen to be as small as possible, subject to keeping the maximum irradiance on any element at $\leq$20 kW/cm^2. Output from the analysis provides all the typical ray-trace data, a plot of the thermal distribution on each element, the thermally induced radii of curvature, and the resultant plots of the x and y OPDs in the cold, hot, and reoptimized hot system. Figure 6(a) illustrates the thermal-distribution plots for the best refractive and reflective cases, respectively. In Figs. 6(b), (c), and (d), OPDs are plotted for the cold, hot, and readjusted hot configuration. Table III summarizes the thermal and OPD data for a range of material values and Table IV lists the calculated adjustment requirements for repptimizing the hot system. Using the more favorable absorption values, either system can be adjusted to operate satisfactorily, but the temperature and thermally induced OPD in fused silica is slightly larger. However, as can be seen in Table III, the higher absorption values for fused silica and sapphire generate OPDs that may be too large to compensate satisfactorily by readjustment. In practice we limit the maximum thermally generated OPD to $\leq$0.2 λ in any single module. This in turn ensures that the component temperatures are low enough to prevent eventual coating damage.

In the reflective configuration, the change in surface temperature at 10^{-5} surface absorption is small (~3^{0} C), corresponding to an almost negligible OPD change in a Zerodur substrate. If the surface absorption is larger or increases due to coating contamination or deterioration, even by an order of magnitude, the low-expansion substrate material and optical configuration are virtually unaffected at the resolution of the calculation. The refractive system requires significant readjustment, even with the superior material properties. Not unexpectedly, a well-designed reflective system is generally more stable and much better suited for high average power operation than a refractive system constructed with the best transmissive materials available today. Nonetheless, the improvements in optical coatings and materials have been significant over the last several years and the average power regime where refractive designs can be used satisfactorily is also correspondingly larger. In any specific application, having a reliable data base on in-system material properties will allow the designer to choose the most cost-effective design.

Astigmatism Correction

Although the reflective design configuration in the example above has a noticeable advantage in thermal stability, an increase in aperture size that would be required at higher power levels can move the reflective telescope into a regime where the geometric aberrations of simple folded optical design more than offset their present advantage in thermal OPD insensitivity. When many optical modules are used in series, geometric,

thermal, and fabrication aberrations can buildup significantly. As part of our optical-design approach, we have developed techniques to compensate for the largest two distortions, focus and astigmatism. The adjustable telescope design can remove spherical or focus errors. In the design, the geometric buildup of astigmatism can be minimized by judicious orientation of successive imaging modules to compensate for cylindrical errors generated in modules near the beginning of the optical train. Unfortunately, perfect cancellation is seldom practical. Fabrication errors also buildup, but with great effort they can be compensated to some degree by judicious rotational orientation of premeasured components. Although each manufacturer has a slightly different polishing technique, the two largest residual fabrication errors are focus and astigmatism. Table V was generated from measuring 29 flat pieces of optics that were manufactured by several vendors and whose maximum dimension ranged from 7.5 to 25 cm. Both the classical aberrations for each piece and the algebraic sum of the appropriate polynomial terms for all 29 pieces fall within the relative ranges indicated in the table. Also included in Table V are the relative peak deformations in each of the next most probable aberrations, coma and spherical aberration, that are required to generate a 0.033 λ rms wave-front aberration. Since astigmatism is clearly the most probable and the most significant distortion affecting the rms wave front after focus is corrected, we have designed as part of the optical train an adjustable cylinder mirror that can be rotated about the optical axis to cancel astigmatism at any arbitrary angle. Proper placement of one or more adjustable cylindrical mirrors minimizes the net overall system

aberration. Figure 7 illustrates the performance of a 10-cm-aperture astigmatism corrector that can add or subtract up to two waves of cylindrical aberration. This relatively simple, easily adjusted mirror assembly has proved to be very effective and clearly provides significant overall improvement in transported beam quality at relatively low cost.

Summary

The design approach described above has been used recently in many of the optical modules used in the LDF optical system at LLNL. Although the static designs developed are only as good as the accuracy of the admittedly approximate calculations, the adaptive features of the system have allowed us to achieve generally good results with a very rapid and flexible design approach. As an indication of its capability, Fig. 8 is a shearing interferogram of a laser beam that has been transported on more than 60 surfaces while being propagated nearly 1 km. Prior to correction for astigmatism the wave-front error was about ($\lambda/4$) rms. After focus and astigmatism were removed, the final wave front had a rms wavefront error of less than ($\lambda/15$). In-system coating performance was also measured yielding an average component transport efficiency greater than 0.995. As the optical and coating design techniques described here are refined, improvements on this performance can be expected.

Use of an adaptive thermo-optical design approach has been very successful in meeting the relatively stringent optical-design criteria of the LDF system. Although this procedure is not well matched to optical

systems requiring very low numerical f-number components, many high-power-laser transport systems have sufficient latitude to work in the regime described above. When this option is available to the designer, this design approach can achieve high overall system performance using configurations that are both inherently insensitive to distortion from thermal loading and are also easily amenable to active reoptimization on both the component and system level.

2942F

References

1. J. I. Davis, J. Z. Holtz, and M. L. Spaeth, "Status and Prospects for Lasers in Isotope Separation," Laser Focus, September, 1982.

2. J. I. Davis and J. A. Paisner, Science, Technology and the Industrialization of Laser-Driven Processes, Lawrence Livermore National Laboratory, Livermore, CA, UCID 20448, (1985).

3. E. I. Moses, "Lawrence Livermore National Laboratory's Atomic Vapor Laser Isotope Separation Program: Laser Technology and Demonstration Facilities," Conference on Lasers and Electro-Optics, p. 182 (May 1985).

4. Optical Design Program developed by Sinclair Optics, Inc., Pittsford, New York, 14534; other programs with similar input provisions would be equally suitable.

5. TSO is not related to a code with the same acronym reported by J. M. Miller, et al., Optical Engineering 20, 1 (1981).

6. V. G. Draggoo, R. G. Morton, R. H. Sawicki, andH. D. Bissinger, "Optical Coating Absorption Measurement for High Power Laser Systems, Proc. SPIE Conf OE LASE, Los Angeles, CA, January 1986.

7. R. T. Swimm, Y. Xiao, and M. Bass, "Calorimetric Study of Optical Absorption of Suprasil W-1 Fused Quartz at Visible, Near IR and Near UV Wavelengths," Appl. Opt.; 24, 322 (1985).

8. R. T. Swimm and M. Bass, private communication (June 1984).

9. T. M. Thomas, "High Laser Damage Threshold Porous Silica Anti-Reflection Coating," submitted to Appl. Opt. (November 1985).

10. J. A. Harrington, B. L. Bobbs, M. Braunstein, R. K. Kim, R. Stearns, and R. Braunstein, "Ultra Violet-Visible Absorption in Highly Transparent Solids by Laser Calorimetry and Wavelength Modulation Spectroscope," Appl. Opt. 17, 1541 (1978).

11. D. A. Pinnow, T. C. Rich, F. W. Ostermayer, Jr., and M. D. Domenico, Jr., "Fundamental Optical Attenuation Limits in the Liquid and Glassy State with Application to Fiber Optical Waveguide Materials," Appl. Phys. Lett. 22, 527 (1973).

12. T. C. Rich and D. A. Pinnow, "Total Optical Attenuation in Bulk Fused Silica," Appl. Phys. Lett. 20, 264 (1972).

13. A. B. Villaverde, R. T. Swimm, and M. Bass, "Calorimetric Measurement of Optical Absorption in Sapphire at Visible, Near IR, and Near UV Wavelengths," NBS Topical Meeting in Basic Properties of Optical Materials, National Bureau of Standards, Washington, DC (May, 1985).

Figure Captions

Fig. 1. Artist's rendering of Laser Demonstration Facility at Lawrence Livermore National Laboratory.

Fig. 2. TSO-OSLO thermo-optical design architecture

Fig. 3. Plot of thermally induced optical-path difference in a radiatively and convectively cooled fused-silica window irradiated with a laser beam having (a) a uniform spatial distribution and (b) the Fresnel diffraction pattern generated by propagating the beam in (a) half way to its far field.

Fig. 4. Compilation of bulk absorption data on fused silica and sapphire plotted as a function of wavelength.

Fig. 5. Optical configuration of imaging module using (A) refractive (lens) elements and (B) reflective (mirror) elements.

Fig. 6. Data summary plots for refractive and reflective telescope designs; (a) Thermal distribution in most highly stressed element; (b) OPD plot of cold optimized system; (c) OPD plot of laser-heated hot system; (d) OPD plot of hot system reoptimized by respacing elements.

Fig. 7. Illustration of the performance of an adjustable cylindrical mirror in removing astigmatism.

Fig. 8. Shearing interferogram of laser beam propagated 1 km through a 60-component optical train.

TABLES

Table I. Specifications of a typical imaging module.

Table II. Thermal input data for mirror and lens systems.

Table III. Summary of temperature and OPD data for several values of surface and bulk absorption.

Table IV. Summary of element spacings for cold and hot telescope configurations in Table III.

Table V. Typical fabrication aberration distribution for 29 flat mirrors including the relative weight of each aberration on the rms wave front..

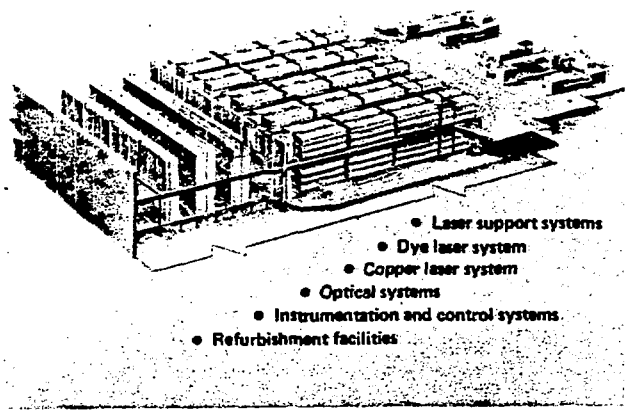
• Laser support systems
• Dye laser system
• Copper laser system
• Optical systems
• Instrumentation and control systems
• Refurbishment facilities

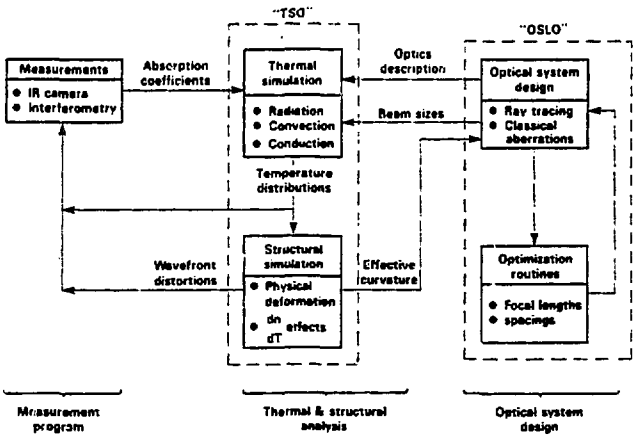
"TSG"
"OSLO"
Measurements
• IR camera
• Interferometry
Absorption coefficients
Thermal simulation
• Radiation
• Convection
• Conduction
Optics description
Optical system design
• Ray tracing
• Classical aberrations
Beam sizes
Temperature distributions
Structural simulation
• Physical deformation
• dn/dT effects
Wavefront distortions
Effective curvature
Optimization routines
• Focal lengths
• spacings
Measurement program
Thermal & structural analysis
Optical system design

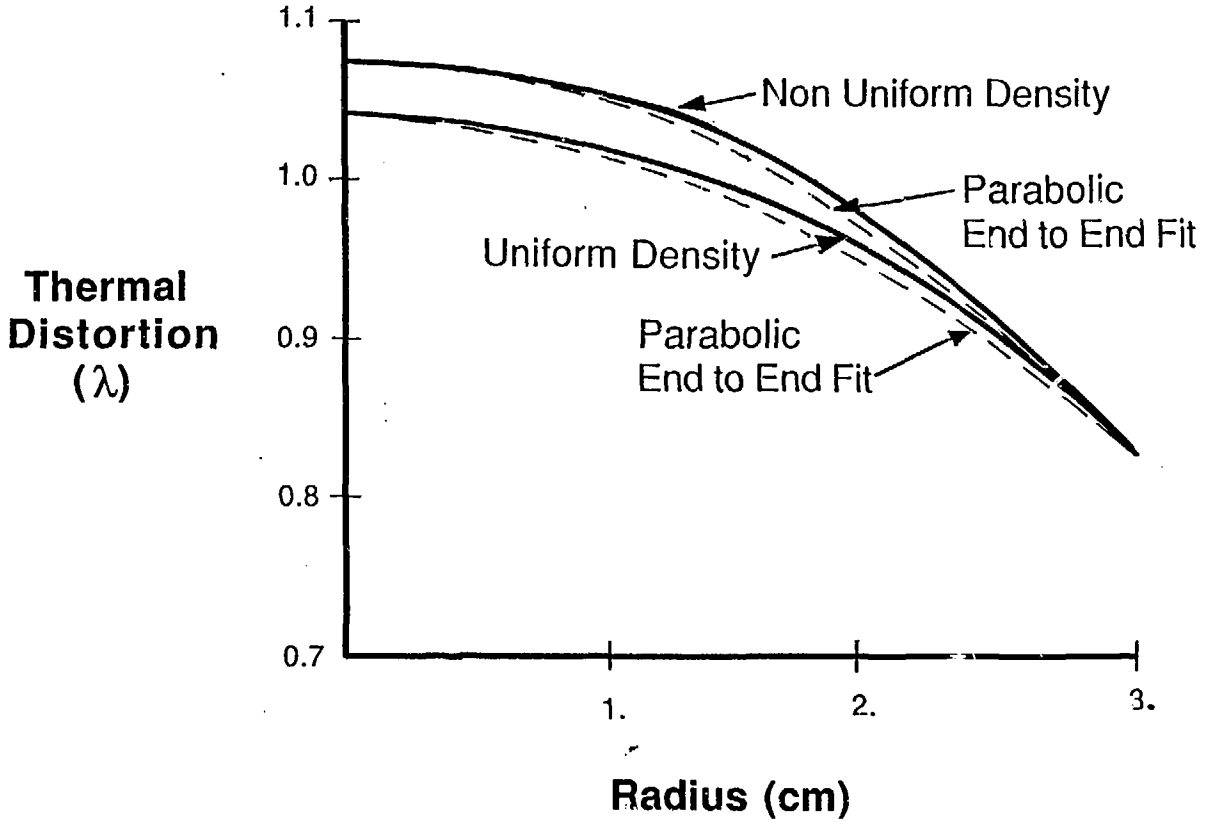
1.1
1.0
0.9
0.8
0.7
Thermal Distortion (λ)
Non Uniform Density
Parabolic End to End Fit
Uniform Density
Parabolic End to End Fit
1.
2.
3.
Radius (cm)

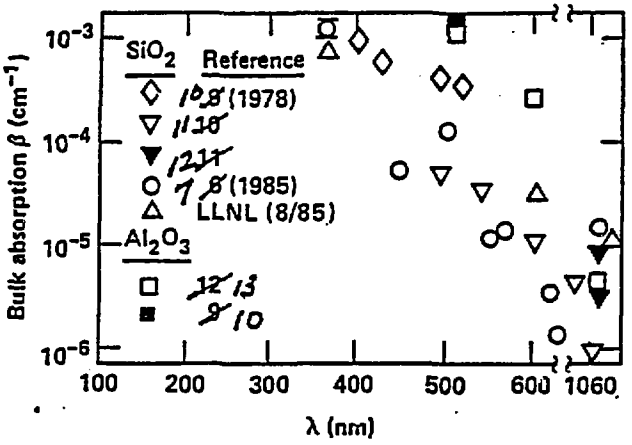

Corrected version due 1/14.

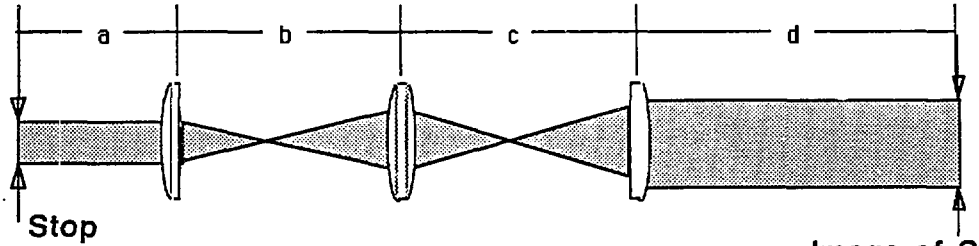

A. Refractive System

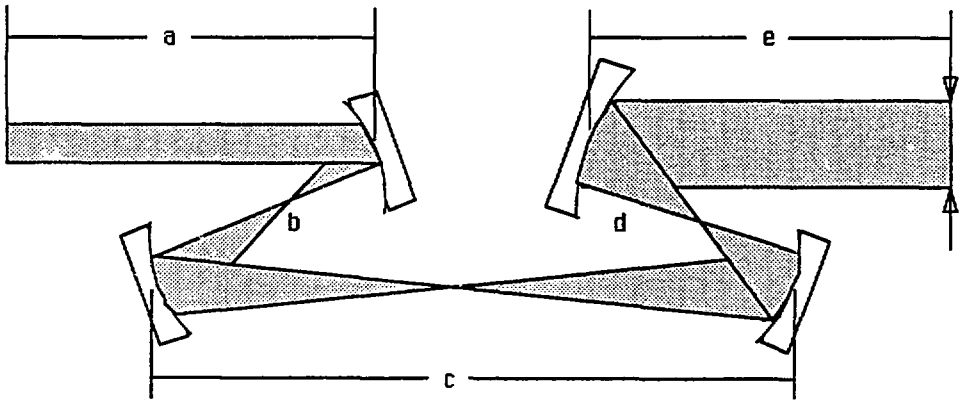

B. Equivalent Reflective System

Reflective System

Refractive System

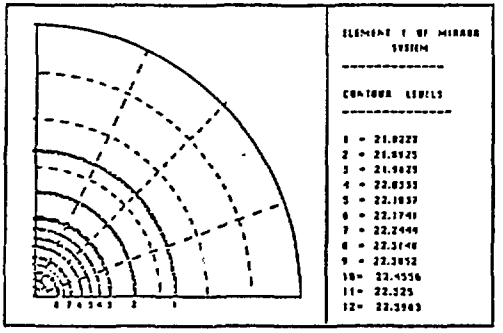

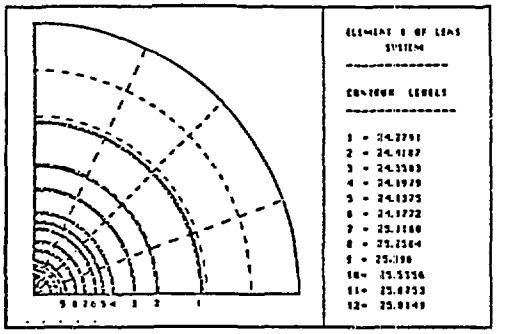

(a)

(b) Cold

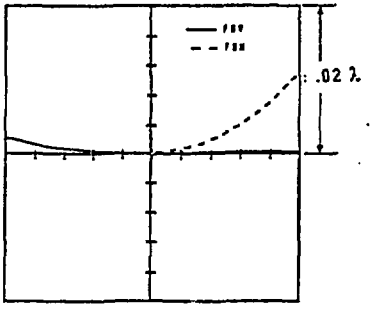

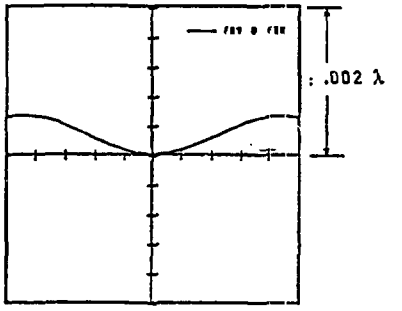

(c) Hot

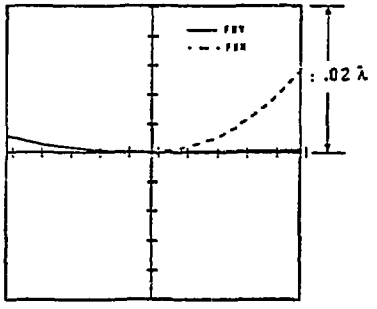

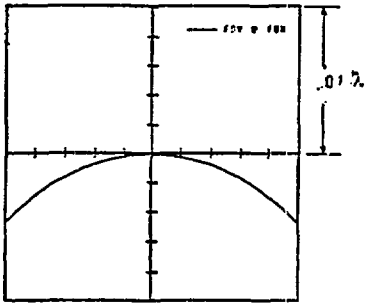

(d) Adjusted Hot

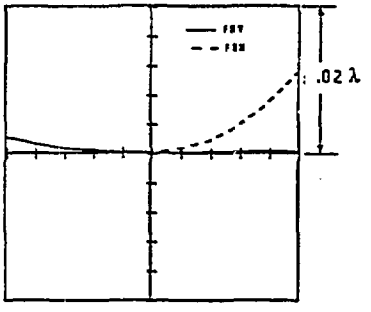

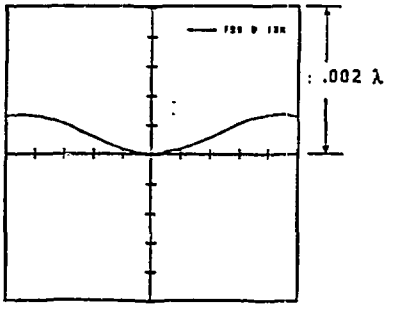

Astigmatic correction

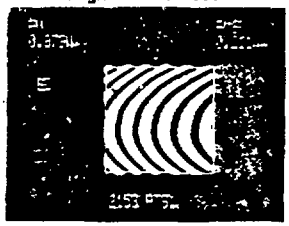

Null adjustment

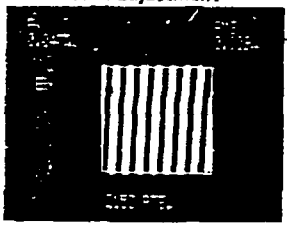

Astigmatism	- 1.001λ
Focus	- 0.047λ
Coma	- 0.026λ
SA3	- 0.035λ

$\Delta\phi_{rms}$ 0.009λ

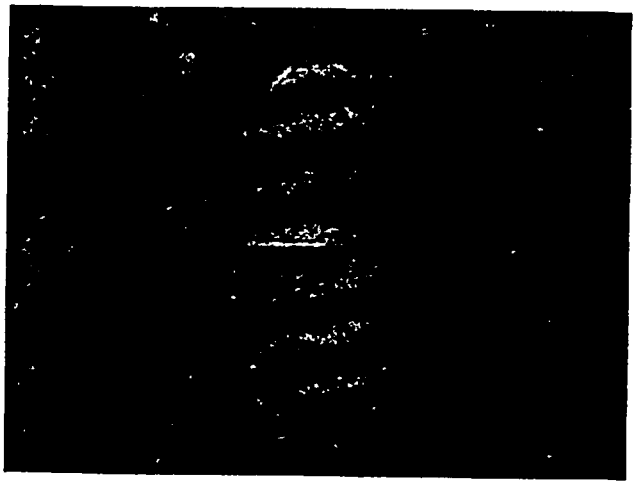

Table I "Typical" optical imaging module specifications

Configuration:	**Afocal imaging telescope with** • **Fixed conjugate distances (≈2 m)** • **Independent adjustment for magnification and collimation**
Input Diameter:	**0.17 cm uniform**
Clear aperture:	**1 cm nominal**
Average power:	**500W**
Maximum design average power density:	**2×10^4 W/cm^2**
Maximum peak geometric aberration (hot and cold):	**$< 0.02\ \lambda$ @ 600 nm**
Net system distortion (hot):	**$< 0.05\ \lambda$/p.p → $< 0.016\ \lambda$rms**

Table II: Thermal input data at 600 nm

Parameters	Materials		
	SiO_2	Al_2O_3	Zerodur
CTE ($^oC^{-1}$)	5.5×10^{-7}	7×10^{-6}	-0.5×10^{-7}
Th. Cond. ($\frac{W}{cm\,^oC}$)	0.014	0.17	0.016
Thermal Emissivity	0.8	0.8	0.8
dn/dt ($^oC^{-1}$)	10^{-5}	1.3×10^{-5}	NA
Bulk absorption (cm^{-1})	5×10^{-4} - 5×10^{-5}	10^{-3}	NA
Coating absorption	10^{-4} - 10^{-5}	10^{-4} - 10^{-5}	10^{-4} - 10^{-5}

Table III Summary of temperature and OPD data for several values of surface and bulk absorption

Telescope Type	Case	Absorption @ 600 nm		Temperature (^{o}C)	OPD (λ)	OPD (λ)
		Surface	Bulk (1^{o}C)			
Transmissive: Fused Silica t=3 mm	A	No heating	No heating	20.0	0.0013	0.0013
	B	10^{-5}	5×10^{-5}	26.0	0.058	0.058
	C	10^{-4}	5×10^{-5}	51.7	0.41	0.41
	D	10^{-4}	5×10^{-4}	65.6	0.64	0.64
Transmissive: Sapphire t= 3 mm	E	No heating	No heating	20.0	0.003	0.003
	F	10^{-5}	10^{-3}	51.0	0.072	0.072
	G	10^{-4}	10^{-3}	65.3	0.13	0.13
Reflective: Zerodur	H	No heating	NA	20.0	0.013	0.0028
	I	10^{-5}	NA	23.0	0.013	0.0028
	J	10^{-4}	NA	36.4	0.013	0.0027

Table IV: Summary of element spacings for cold and hot telescope configurations in Table III

	Spacings (mm)	a	b	c	d	e
A	Silica Lenses	342	519	474	644	
B		338	516	474	651	
C		313	502	472	692	*
D		300	495	471	714	*
E	Sapphire Lenses	342	519	474	645	
F		337	517	474	654	
G		333	514	474	661	
H	Mirror System	761	419	1309	419	745
I		761	419	1309	419	745
J		765	419	1312	419	737

* Validity of cases uncertain

TABLE 5

Optical system performance tolerance to typical aberrations

Aberration	Functional form	Max value @ $\Delta\Phi \leqslant (\lambda/30)$rms	Relative occurrence in fabricated optics
Defocus	$A_{020}\,\rho^2$		1.00
Astigmatism	$A_{022}\,\rho^2\cos^2\theta$	$\lvert A_{022}\rvert \lesssim 0.28\lambda$	0.40 - 0.60
Coma	$A_{031}\,\rho^3\cos\theta$	$\lvert A_{031}\rvert \lesssim 0.49\lambda$	0.05 - 0.20
Spherical	$A_{040}\,\rho^4$	$\lvert A_{040}\rvert \lesssim 0.76\lambda$	0.05 - 0.10